# A Short-Term Spatio-Temporal Approach for Photovoltaic Power Forecasting

Akin Tascikaraoglu*, Borhan M. Sanandaji†, Gianfranco Chicco‡, Valeria Cocina‡
Filippo Spertino‡, Ozan Erdinc*, Nikolaos G. Paterakis§ and João P. S. Catalão¶

* Yildiz Technical University, Istanbul, Turkey
{atasci,oerdinc}@yildiz.edu.tr
† University of California, Berkeley, CA, USA
sanandaji@eecs.berkeley.edu
‡ Politecnico di Torino, Torino, Italy
{gianfranco.chicco,valeria.cocina,filippo.spertino}@polito.it
§ Eindhoven University of Technology, Eindhoven, The Netherlands
n.paterakis@tue.nl
¶ FEUP, Porto, UBI, Covilhã, and INESC-ID, IST, Univ. of Lisbon, Lisbon, Portugal
catalao@ubi.pt

*Abstract*—This paper presents a Photovoltaic (PV) power conversion model and a forecasting approach which uses spatial dependency of variables along with their temporal information. The power produced by a PV plant is forecasted by a PV conversion model using the predictions of three weather variables, namely, irradiance on the tilted plane, ambient temperature, and wind speed. The predictions are accomplished using a *spatio-temporal* algorithm that exploits the sparsity of correlations between time series data of different meteorological stations in the same region. The performances of the forecasting algorithm as well as the PV conversion model are investigated using real data recorded at various locations in Italy. The comparisons with various benchmark methods show the effectiveness of the proposed approaches over short-term forecasts.

*Index Terms*—Forecasting; Solar irradiance; Distributed generation; Correlated data; Time series.

## I. INTRODUCTION

Integration of renewable energy sources into the power grid is greatly facilitated by high-accuracy forecasts. Using historical data of a variable in a prediction model can generally provide a reasonable forecast accuracy [1]. In order to further improve the forecast performance, however, spatial information can also be used in addition to the temporal data. High correlations between the weather variables such as solar irradiance, temperature and wind speed among neighboring sites mostly can help improve the forecast accuracy. However, incorporating various time series data over a large number of meteorological stations is generally challenging due to the

overfitting problems and computational costs. Therefore, the optimum amount of data to be included in the forecasting process without affecting the prediction performance has to be determined by using advanced algorithms.

Recently, there has been an increasing number of studies using spatial information in solar forecasting methods. Dambreville et al. [2] propose an Autoregressive (AR) approach to predict the global horizontal irradiance by using spatio-temporal information. Another time series model, an Auto Regressive with eXternal input (ARX) model, is proposed for solar PV power forecast depending on correlated power information from different stations [3]. A Neural Network (NN) approach based on spatio-temporal information is employed by Licciardi et al. [4] for global horizontal irradiance forecasts, where also Principal Component Analysis (PCA) is used to decrease the computational load. Agoua et al. [5] use distributed power plants as sensors in a spatio-temporal approach by only taking the production data into account. Besides, spatio-temporal forecasting methods based on vector autoregression are presented for solar power forecasts [6] and very short term wind power forecasts [7], by considering the past observations only from the related variable, i.e, solar power data and wind power data, respectively. A more detailed survey of solar irradiance forecasting approaches based on spatial and temporal information can be found in [8] and [9].

Considering the promising results presented, this paper proposes a forecasting scheme which uses both spatial and temporal time series data. The proposed *spatio-temporal* forecasting algorithm incorporates the time series data of a target meteorological station and its surrounding stations. Assuming that there usually exists a sparse relational pattern among the correlations between the time series of relatively close meteorological stations (i.e., only a few stations have a strong correlation with the target station among a set of stations), we study how to determine such low-dimensional structures

and then using them in forecasting in order to improve the accuracy while decreasing the computational burden. With this objective, first, we show that under the assumption of *sparsity* of the interconnections, there is a distinct structure to the solution $x$. It is assumed that a coefficient vector $x$ has very few non-zero entries, and these entries are clustered in few certain locations. The number of blocks in this *block-sparse* coefficient vector corresponds to the number of links (i.e., stations) contributing to the target station output.

Using the proposed model structure, called Compressive Spatio-Temporal Forecasting (CSTF), as it is inspired by Compressive Sensing (CS) and structured-sparse recovery [10], [11], the forecasts are performed for three different weather variables, namely, irradiance on the tilted plane, ambient temperature and wind speed. The forecast values are then applied to a PV power conversion model [12] in order to estimate the output power produced by a PV plant. It is also to be noted that various exogenous variables are incorporated in forecasting, by determining the variable type with a cross-correlation analysis between the variables. For instance, temperature and humidity values are used for irradiance forecasts while temperature, pressure and wind direction series are included in wind speed forecasts. The performance of both the PV conversion model and the spatio-temporal algorithm are evaluated on a yearly basis using high-resolution real data recorded in various locations in Italy and the results are compared to a set of widely-used temporal and spatio-temporal benchmark models.

The remainder of the paper is organized as follows: Section II presents the PV system and PV conversion model. In Section III, the proposed forecasting algorithm is introduced in Section IV. The comparisons with the real data and with the other benchmark methods are given in Section V. The last section contains the conclusion.

## II. ELECTRIC POWER EVALUATION

For the calculations reported in this paper, data are taken from a meteorological station installed in a grid-connected PV system located in Southern Italy. The plant is facing South and the tilt angle of the poly-crystalline silicon modules is $30°$. With a peak power of 993.6 $kW_p$, the plant utilizes two centralized transformerless inverters, slightly undersized with respect to the rated peak power, given that the 500-$kVA$ inverter is supplied by a 552 $kW_p$ array and the 400-$kVA$ inverter is supplied by a 441.6 $kW_p$ array, respectively. A complete description of the system is reported in [13].

In order to link the solar irradiance and the cell temperature data with the AC power delivered to the grid, a dedicated PV conversion model is defined. The available power in the maximum power point $P_{mpp}$, is achieved by:

$$P_{mpp} = P_{rated} \cdot (G_{tcell} - G_{lim}) \cdot \eta_{dirt} \cdot \eta_{refl} \cdot \eta_{th} \cdot \eta_{mism} \cdot \eta_{cable} \quad (1)$$

where:

- $P_{rated}$ is the rated (a.k.a. peak) power of the real grid-connected PV system at Standard Test Conditions (STC);

- $G_{lim}$ is the irradiance limit below which the output is vanishing;
- $G_{tcell}$ is the global irradiance of a $30°$ tilted reference solar cell;
- $\eta_{dirt}$ is the efficiency due to soiling and dirt losses, the corresponding value used is in the range 0.97 - 0.98;
- $\eta_{refl}$ is the efficiency due to the reflection of the PV module glass, the corresponding value used is taken from the PVGIS website and equal to 0.971 [14];
- $\eta_{th}$ is the efficiency due to the thermal losses $\ell_{th}$ with respect to the STC, calculated as a function of the thermal coefficient of maximum power of the modules $\gamma_{th}$, which depends on the PV technology, and the cell temperature $T_C$, which can be calculated as:

$$T_C = T_{amb} + (NOCT - 20°) \cdot G_{tcell}/0.8kW/m^2 \quad (2)$$

where $T_{amb}$ is the ambient temperature and $NOCT$ is the Normal Operating Cell Temperature in outdoor operation ($G_{NOCT}$ = 800 $W/m^2$ and $T_{amb}$ = 20°C), whose value is in the range 42-50°C) [15].
- $\eta_{mism}$ is the efficiency that takes into account the *I-V* mismatch losses assuming that the bottleneck effect globally leads to 97% of the power rating declared by the manufacturer for all the PV modules in the PV array. This loss is a consequence of the weakest modules in the series connection inside the strings and of the weakest strings in the parallel connection inside the PV array [16];
- $\eta_{cable}$ is the efficiency that includes the DC cable losses with value 0.99, according to good design criteria [17].

Finally, considering the efficiency of the maximum power point tracker, $\eta_{MPPT}$, and thanks to the power conditioning unit model for grid connection, the AC power injected into the grid is calculated as [18]:

$$P_{DC} = \eta_{MPPT} \cdot P_{mpp} \quad (3)$$

$$P_{AC} = P_{DC} - \left(P_0 + c_Q \cdot P_{AC}^2\right) \quad (4)$$

where $P_0$ is the no-load power losses along the operation (equal to 0.21% of the 552 $kW_p$ AC rated power and 0.23% of the 441.6 $kW_p$ AC rated power) and $c_Q$ is the quadratic loss coefficients (with $c_Q P_{AC}^2$ equal to 1.9% of the 552 $kW_p$ AC rated power and 1.8% of the 441.6 $kW_p$ AC rated power).

For above calculations, $T_{amb}$ and $G_{tcell}$ are taken from the forecasts and used to determine the AC power $P_{AC}$.

## III. MULTIVARIATE AUTOREGRESSIVE (M-AR) MODEL

We use M-AR models to represent the interactions between time series data of different stations as follows:

$$\begin{aligned} \boldsymbol{y}(t) &= \boldsymbol{X}_1\boldsymbol{y}(t-1) + \cdots + \boldsymbol{X}_n\boldsymbol{y}(t-n) + \boldsymbol{e}(t) \\ &= \sum_{j=1}^{n} \boldsymbol{X}_j\boldsymbol{y}(t-j) + \boldsymbol{e}(t), \end{aligned} \quad (5)$$

where $\boldsymbol{y}(t) \in \mathbb{R}^P$ contains output measurements (e.g., irradiance values at $P$ meteorological stations) at time $t$, $\boldsymbol{X}_j \in$

$$
\underbrace{\begin{bmatrix} y_{n+1}^{v^\star,s^\star} \\ y_{n+2}^{v^\star,s^\star} \\ \vdots \\ y_{n+M}^{v^\star,s^\star} \end{bmatrix}}_{\boldsymbol{b}\in\mathbb{R}^M} = \underbrace{\left[ \begin{array}{ccc|ccc|ccc} y_n^{1,1} & \cdots & y_1^{1,1} & \cdots & \cdots & & y_n^{V,S} & \cdots & y_1^{V,S} \\ y_{n+1}^{1,1} & \ddots & \vdots & & & & y_{n+1}^{V,S} & \ddots & \vdots \\ \vdots & \ddots & \vdots & & & \cdots & \vdots & & \vdots \\ y_{n+M-1}^{1,1} & \cdots & y_M^{1,1} & \cdots & \cdots & & y_{n+M-1}^{V,S} & \cdots & y_M^{V,S} \end{array} \right]}_{\boldsymbol{A}\in\mathbb{R}^{M\times N}} \underbrace{\begin{bmatrix} \left.\begin{matrix} x_1^{1,1} \\ \vdots \\ x_n^{1,1} \end{matrix}\right\} \text{Block 1} \\ \hline \vdots \\ \vdots \\ \hline \left.\begin{matrix} x_1^{V,S} \\ \vdots \\ x_n^{V,S} \end{matrix}\right\} \text{Block } P \end{bmatrix}}_{\boldsymbol{x}\in\mathbb{R}^N} \tag{6}
$$

$\mathbb{R}^{P\times P}$ is a coefficient matrix associated with the $j$-th time lag, $n$ is the model order and $\boldsymbol{e}(t)$ is a Gaussian noise.

Let's assume that data is obtained from $V$ weather variables ($v = 1, 2, \ldots, V$) recorded at $S$ locations ($s = 1, 2, \ldots, S$). Define $y_t^{s,v}$ as the measured value of the $v$-th variable at the $s$-th location at sample time $t$ ($t = 1, 2, \ldots, M + n$). For the target variable $y^{s^*,v^*}$, the M-AR model (5) can be expressed in a matrix-vector product format as in (6), where $N := nP$ and $P := V \times S$. In the training phase, the goal is to determine a coefficient vector $\boldsymbol{x} \in \mathbb{R}^N$ that best explains the observations $\boldsymbol{b} \in \mathbb{R}^M$ and $\boldsymbol{A} \in \mathbb{R}^{M\times N}$. As seen from (6), the coefficients belonging to each variable appear in one vector-block.

## IV. COMPRESSIVE SPATIO-TEMPORAL FORECASTING

The proposed forecasting structure depends on the assumption that only a few meteorological stations have a strong correlation with the target station among a set of stations. Under this assumption, there will be a distinct structure to the solution $\boldsymbol{x}$. In particular, a typical $\boldsymbol{x}$ will have very few non-zero entries clustered in few locations. Such vectors are called *block-sparse*. Each block represents a link contributing to the output of the target station. For a given target meteorological station, we solve the minimization:

$$\min_{\boldsymbol{x}} \|\boldsymbol{b} - \boldsymbol{A}\boldsymbol{x}\|_2 \quad \text{subject to} \quad (\boldsymbol{x} \text{ is block-sparse}). \tag{7}$$

We use tools from CS for solving (7).

### A. Uniform CSTF

*Definition 1 (Block K-Sparse Signal):* Let $\boldsymbol{x} \in \mathbb{R}^N$ be a concatenation of $P$ vector-blocks $\boldsymbol{x}_i \in \mathbb{R}^n$, i.e.,

$$\boldsymbol{x} = [\boldsymbol{x}_1^{\text{tr}} \cdots \boldsymbol{x}_i^{\text{tr}} \cdots \boldsymbol{x}_P^{\text{tr}}]^{\text{tr}}, \tag{8}$$

where $N = nP$. A signal $\boldsymbol{x} \in \mathbb{R}^N$ is called *block K-sparse* if it has $K < P$ non-zero blocks. $\square$

Among different algorithms for block-sparse recovery, we use the Block Orthogonal Matching Pursuit (BOMP) algorithm [19] due to its flexibility in recovering block-sparse signals of different sparsity levels and its low computation complexity [20]. For more details on BOMP, see [21].

### B. Nonuniform CSTF

In a uniform CSTF, the assumption is that a uniform M-AR model as given in (6) is governing the interactions between meteorological stations. In other words, we assume that the target station and its surrounding stations are related by AR models of the same order. In this section, we consider a more generalized version of the CSTF algorithm where the target station and its surrounding stations are related by AR models of different orders. This model structure, called Nonuniform Multivariate Autoregressive (NM-AR), distinguishes between the stations with high and low cross-correlation with the target station. Let $n_i$ be the order associated with the $i$-th station for $i = 1, 2, \ldots, P$. An NM-AR version of (6) can be considered as given in (9), where $n_{\max} \geq \max_i n_i$ and $N := \sum_{i=1}^P n_i$. This model structure results in a nonuniform block-sparse vector $\boldsymbol{x}$ whose blocks have different length.

*Definition 2 (Nonuniform Block K-Sparse Signal):* Let $\boldsymbol{x} \in \mathbb{R}^N$ as a concatenation of $P$ vector-blocks $\boldsymbol{x}_i \in \mathbb{R}^{n_i}$ where $N = \sum_{i=1}^P n_i$. A signal $\boldsymbol{x} \in \mathbb{R}^N$ is called *nonuniform block K-sparse* if it has $K < P$ non-zero blocks. $\square$

Given $\{n_i\}_{i=1}^P$, the BOMP Algorithm can be used for recovery of $\boldsymbol{x}$ with $\boldsymbol{A}_i \in \mathbb{R}^{M\times n_i}$. In order to find the set of order $\{n_i\}_{i=1}^P$, we use a correlation analysis in which the correlation coefficients for the consecutive time lags up to the prediction horizon between the target and other stations are calculated. We adjust the orders to achieve the best prediction performance based on the calculated correlation coefficients.

## V. CASE STUDY OF FIVE STATIONS IN ITALY

The variables $G_{tcell}$, $T_{amb}$, and $w_s$ measured at five meteorological stations in Italy are used in the the proposed CSTF algorithm. These stations face high solar irradiance values during a large part of the year and hence, are good candidates for our case studies. Furthermore, these stations are located in a relatively small region, as shown in Fig. 1, making them attractive candidates for correlated data analysis.

### A. Data Description

Data averaged each 10 min from five meteorological stations in Italy including Ga1, Ga2, Gi, Ma and Ru are used in

$$
\underbrace{\begin{bmatrix} y^{v^\star,s^\star}_{n_{\max}+1} \\ y^{v^\star,s^\star}_{n_{\max}+2} \\ \vdots \\ y^{v^\star,s^\star}_{n_{\max}+M} \end{bmatrix}}_{\boldsymbol{b}\in\mathbb{R}^M} = \underbrace{\begin{bmatrix} y^{1,1}_{n_{\max}} & \cdots & \cdots & \cdots & y^{1,1}_{n_{\max}-n_1+1} & \cdots & y^{V,S}_{n_{\max}} & \cdots & y^{V,S}_{n_{\max}-n_P+1} \\ y^{1,1}_{n_{\max}+1} & \ddots & \ddots & \ddots & \vdots & & y^{V,S}_{n_{\max}+1} & \ddots & \vdots \\ \vdots & \ddots & \ddots & \ddots & \vdots & & \vdots & \ddots & \vdots \\ y^{1,1}_{n_{\max}+M-1} & \cdots & \cdots & \cdots & y^{1,1}_{n_{\max}-n_1+M} & \cdots & y^{V,S}_{n_{\max}+M-1} & \cdots & y^{V,S}_{n_{\max}-n_P+M} \end{bmatrix}}_{\boldsymbol{A}\in\mathbb{R}^{M\times N}} \underbrace{\begin{bmatrix} x^{1,1}_1 \\ \vdots \\ \vdots \\ \vdots \\ x^{1,1}_{n_1} \\ \hline \vdots \\ \hline x^{V,S}_1 \\ \vdots \\ x^{V,S}_{n_P} \end{bmatrix}}_{\boldsymbol{x}\in\mathbb{R}^N} \left.\begin{matrix} \\ \\ \\ \end{matrix}\right\} \text{Block 1} \quad \left.\begin{matrix} \\ \\ \end{matrix}\right\} \text{Block } P
$$

(9)
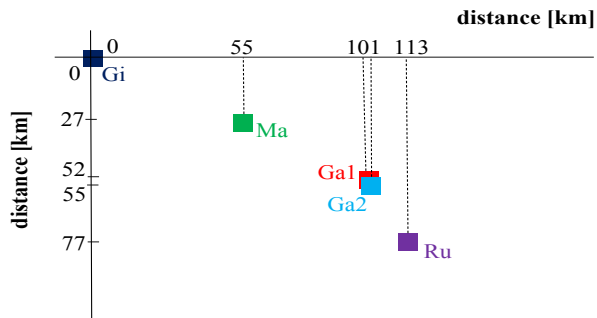


Figure 1. Map of the five PV plants.

TABLE I. STATISTICAL PARAMETERS OF THE DATA USED IN THE TEST PERIODS.

| Period | Mean [$W/m^2$] | Median [$W/m^2$] | Standard Deviation [$W/m^2$] |
|---|---|---|---|
| **February 1-7** | 69.82 | 0.00 | 355.71 |
| **July 1-7** | 293.69 | 74.34 | 142.75 |

the study. To clearly observe the forecasting performance, the variables $G_{tcell}$, $T_{amb}$ and $w_s$ belonging to the target station Gi are forecasted separately for two representative time periods; first week of February and the first week of July. For each period, periods of 14 and 7 days from previous months (i.e., January and June) are also considered as training and model selection subsets, respectively. The results are presented in the related figures and tables for only the irradiance data due to several reasons: (i) similar forecasting performances for the variables cause data redundancy, (ii) solar irradiance is the most influencing variable on the power calculations and, (iii) directly providing power forecasts instead of irradiance forecasts does not allow to make fair comparisons with the forecasting methods in the literature since power forecasts in this study include the contributions of different variables on the accuracy and also the errors coming from the forecasts of these variables and the model itself.

The main descriptive statistics belonging to irradiance values in the selected representative weeks are given in Table I. The highly volatile data characteristics in these periods, complicates the forecasting task, allowing the performance of proposed model to be tested at the worst conditions.

### B. Comparison with Other Benchmark Algorithms

The proposed algorithm is compared with a set of forecasting approaches for two periods of seven consecutive days

with one hour-ahead (i.e. six 10-min-ahead) updates. First, a *persistence* model is considered due to its high performance in short-term forecasts. The persistence model uses the last measured value for the prediction of the next six time steps. Then an AR model is employed. As seen in Figs. 2 and 3, the AR model outperforms the persistence model.

A combination method consisting of Wavelet Transform (WT) and Artificial Neural Network (ANN) [22] is also used for comparison. In this model, briefly, the solar irradiance on tilted plane data is decomposed by the WT into three subseries at various frequency bands and each subseries is forecasted separately using ANN before an aggregation process. The final forecast, shown in Fig. 4, outperforms the AR model due to ANN's capability of capturing the existing nonlinearity. Decomposition models are in general proved to improve the forecasting accuracy [23]. In addition to the temporal methods, a Least Squares (LS) M-AR spatio-temporal forecasting model is employed. Fig. 5 shows the improved forecasting results.

### C. Nonuniform CSTF

Lastly, the proposed nonuniform CSTF algorithm is applied to the considered data set. As indicated before, the simulations are carried out for a prediction time horizon of one hour, hence a new coefficient vector $\boldsymbol{x}$ is calculated every one hour, i.e. every six 10-min time steps. In the forecasting stage, a recursive approach is adopted. In other words, the forecasts at time $n+M+1$ for all meteorological stations ($\hat{y}^i_{n+M+1}, \forall i$) are included in the $\boldsymbol{A}$ matrix for forecasting the solar irradiance at time $n+M+2$ ($\hat{y}^i_{n+M+2}, \forall i$) and so on. This process continues for six time steps and the elements of $\boldsymbol{A}$ matrix are updated with measured values for each prediction time horizon.
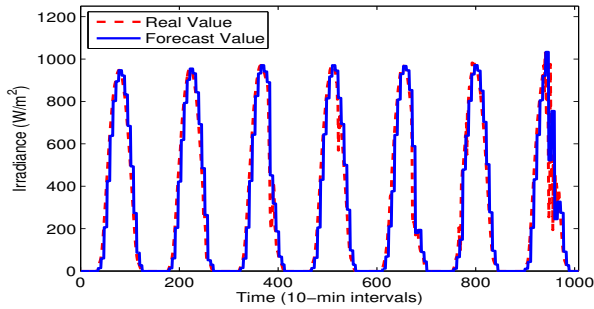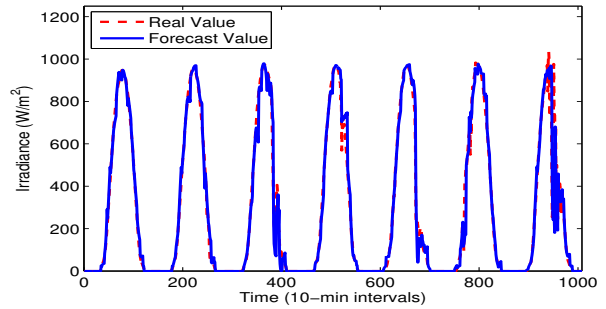
(a) Summer
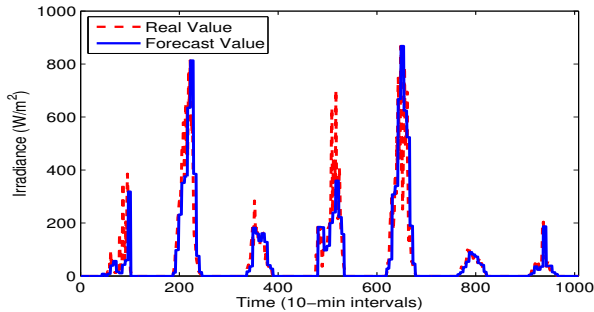


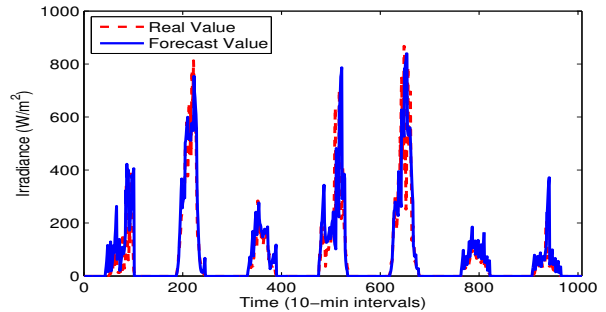(b) Winter

Figure 2. Persistence forecasting of two data sets.



(a) Summer



(b) Winter
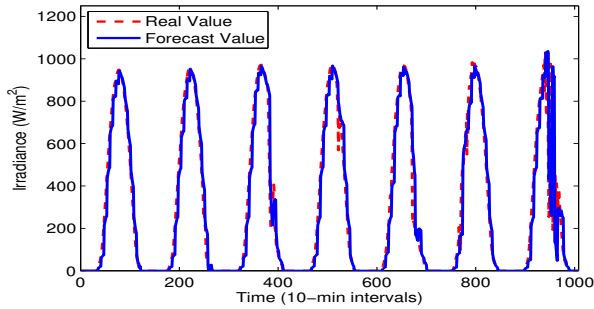
Figure 3. AR forecasting of two data sets.



(a) Summer

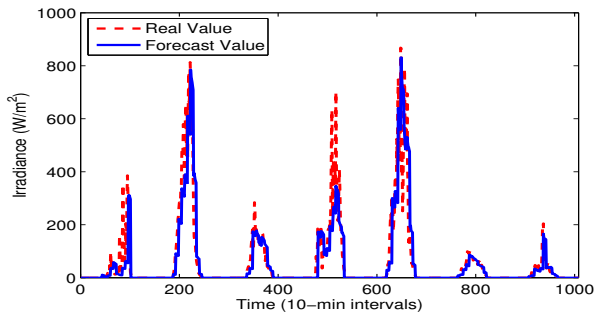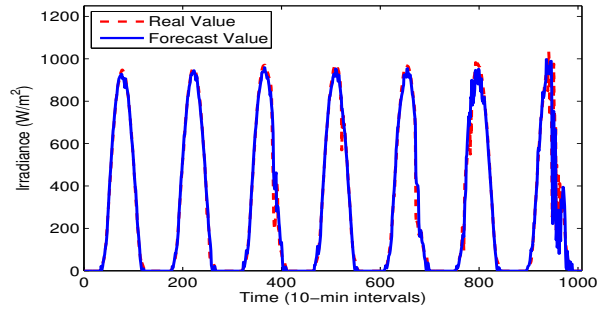

(b) Winter

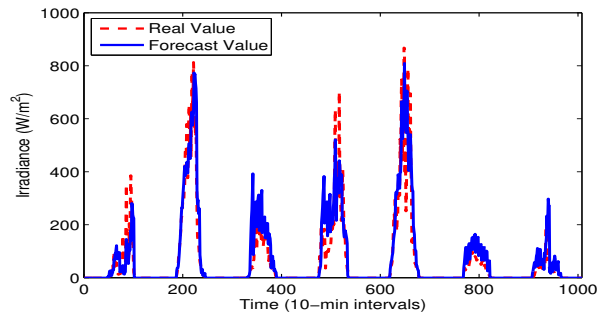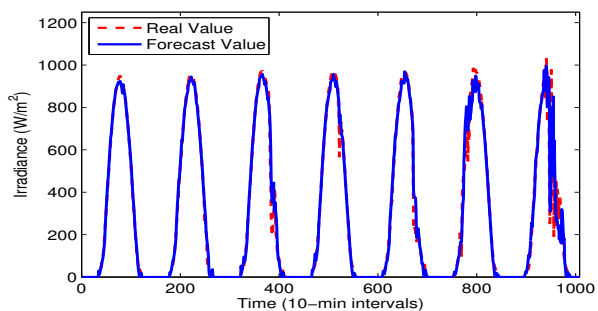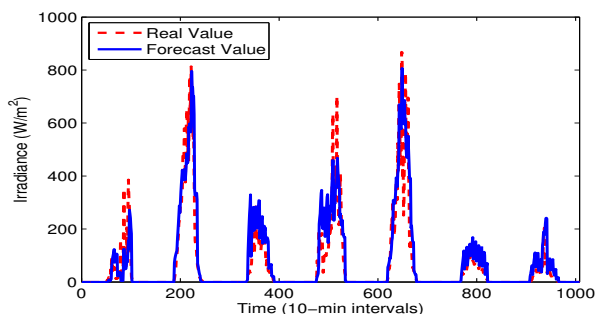Figure 4. WT-ANN forecasting of two data sets.



(a) Summer



(b) Winter

Figure 5. LS M-AR forecasting of two data sets.

As depicted in Fig. 6, substantially improved forecasting accuracy for two considered data sets are achieved compared to both temporal and spatio-temporal methods. In Table II, averaged Mean Absolute Error (MAE), Root Mean Squared Error (RMSE) and Normalized Root Mean Squared Error (NRMSE) metrics are provided for a comparison between the methods considered in this study for both weeks. The proposed nonuniform CSTF algorithm outperforms the other
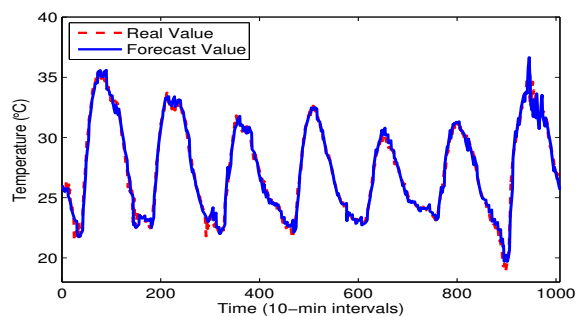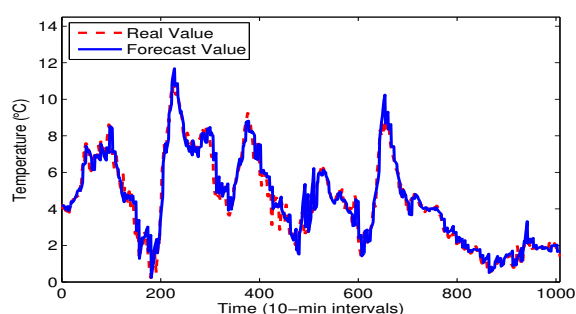
(a) Summer



(b) Winter

Figure 6. Nonuniform CSTF forecasting of two data sets.



(a) Summer



(b) Winter

Figure 7. Nonuniform CSTF forecasting of two temperature data sets.

approaches with respect to all error metrics. Considering the NRMSE values as an example, the proposed approach enables a reduction of 14.20% and 6.04% as compared to the WT-ANN and LS-based ST, respectively.

TABLE II.    STATISTICAL ERROR MEASURE COMPARISON OF DIFFERENT

METHODS

| Forecasting approach | MAE $[W/m^2]$ | RMSE $[W/m^2]$ | NRMSE [%] |
|---|---|---|---|
| **Persistence Forecasting** | 53.28 | 110.59 | 9.32 |
| **AR** | 31.54 | 89.97 | 7.58 |
| **WT-ANN** | 21.68 | 75.26 | 6.34 |
| **LS-based ST** | 19.22 | 68.72 | 5.79 |
| **Nonuniform CSTF** | 18.48 | 64.56 | 5.44 |

Note that the exogenous variables are included in the proposed model structure. The weather variables, temperature, and humidity are incorporated for solar irradiance forecasts to benefit from the high correlations between solar irradiance and these variables. Besides, irradiance, humidity, and wind direction are included in temperature forecasts, and temperature and wind direction are used for wind speed forecasts. The type and order of the variables to be incorporated as inputs are chosen by examining the cross-correlations between the variables.

### D. PV Power Predictions

In order to estimate the solar power values, the variables ambient temperature and wind speed are also predicted with the modified CSTF algorithm, as illustrated in Figs. 7 and 8. The averaged NRMSE values of 4.42% and 9.69% are obtained
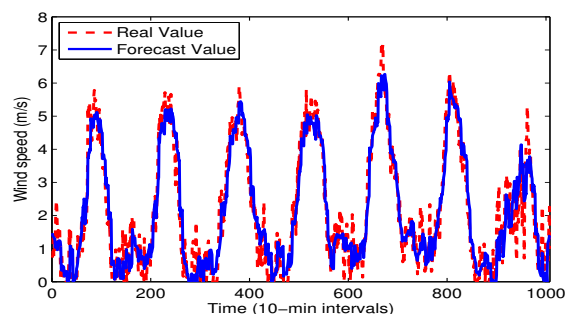


(a) Summer
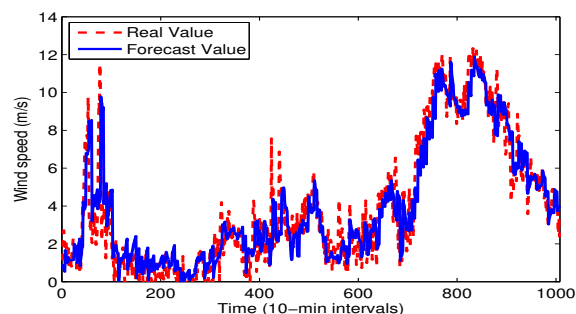


(b) Winter

Figure 8. Nonuniform CSTF forecasting of two wind speed data sets.

for temperature and wind speed, respectively. Eventually, the output power produced by the PV plant is calculated by applying all the forecasted data to the power conversion model. Thanks to the proposed forecasting and power conversion
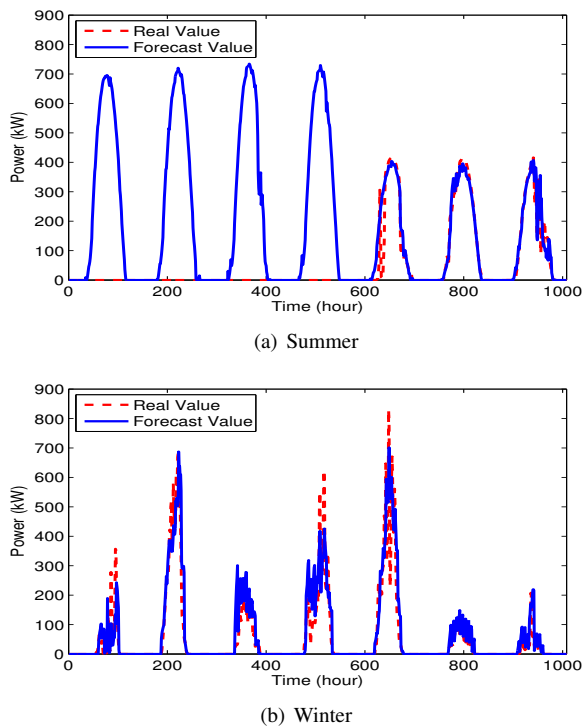
(a) Summer



(b) Winter

Figure 9. Nonuniform CSTF forecasting of two power data sets.

models, the results that are mostly consistent with the real data are accomplished as seen in Fig. 9. The calculated error measures for the power forecasts, an RMSE of 45.95 $kW$ and a NRMSE of 5.79%, confirm the effectiveness of the proposed models. It is to be emphasized again that the superiority of the models mainly comes from exploiting all available data in an effective and computationally efficient way. It is also noted that the computational time of the proposed model is almost negligible, which is about 0.2 seconds for each 6 steps in the MATLAB environment on a standard desktop computer.

## VI. CONCLUSION

A spatio-temporal solar power forecasting approach and a PV power conversion model are proposed in this paper. First the short-term forecasts of different weather variables are achieved with high accuracy using the proposed forecasting strategy that incorporates the time series data of both a target meteorological station and its surrounding stations. The PV power conversion model uses these forecasts to calculate the estimated output power produced by a PV plant. Compared to a set of benchmark models, the lowest error metrics are obtained for the proposed approach proving its efficiency in short-term forecasting. The power forecasts also validate the modeling accuracy of the PV power conversion model.

## REFERENCES

[1] A. Tascikaraoglu, A. Boynuegri, and M. Uzunoglu, "A demand side management strategy based on forecasting of residential renewable sources: A smart home system in turkey," *Energy and Buildings*, vol. 80, pp. 309–320, 2014.

[2] R. Dambreville, P. Blanc, J. Chanussot, and D. Boldo, "Very short term forecasting of the global horizontal irradiance using a spatio-temporal autoregressive model," *Renewable Energy*, vol. 72, pp. 291–300, 2014.

[3] C. Yang, A. Thatte, and L. Xie, "Multitime-scale data-driven spatio-temporal forecast of photovoltaic generation," *IEEE Transactions on Sustainable Energy*, vol. 6, pp. 104–112, 2015.

[4] G. Licciardi, R. Dambreville, J. Chanussot, and S. Dubost, "Spatiotemporal pattern recognition and nonlinear pca for global horizontal irradiance forecasting," *Geoscience and Remote Sensing Letters*, vol. 12, pp. 284–288, 2015.

[5] X. G. Agoua, R. Girard, and G. Kariniotakis, "Spatio-temporal models for photovoltaic power short-term forecasting," in *Solar Integration workshop 2015*, 2015.

[6] R. J. Bessa, A. Trindade, and V. Miranda, "Spatial-temporal solar power forecasting for smart grids," *Industrial Informatics, IEEE Transactions on*, vol. 11, no. 1, pp. 232–241, 2015.

[7] J. Dowell and P. Pinson, "Very-short-term probabilistic wind power forecasts by sparse vector autoregression," *IEEE Transactions on Smart Grid*, vol. 7, pp. 763–770, 2016.

[8] M. Diagne, M. David, P. Lauret, J. Boland, and N. Schmutz, "Review of solar irradiance forecasting methods and a proposition for small-scale insular grids," *Renewable and Sustainable Energy Reviews*, vol. 27, pp. 65–76, 2013.

[9] J. Boland, "Spatial-temporal forecasting of solar radiation," *Renewable Energy*, vol. 75, pp. 607–616, 2015.

[10] B. M. Sanandaji, A. Tascikaraoglu, K. Poolla, and P. Varaiya, "Low-dimensional models in spatio-temporal wind speed forecasting," in *American Control Conference (ACC), 2015*. IEEE, 2015, pp. 4485–4490.

[11] A. Tascikaraoglu, B. M. Sanandaji, K. Poolla, and P. Varaiya, "Exploiting sparsity of interconnections in spatio-temporal wind speed forecasting using wavelet transform," *Applied Energy*, vol. 165, pp. 735–747, 2016.

[12] V. Cocina, "Economy of grid-connected photovoltaic systems and comparison of irradiance / electric power predictions vs. experimental results," Ph.D. dissertation, Politecnico di Torino, Italy, 2014.

[13] G. Chicco, V. Cocina, P. Di Leo, and F. Spertino, "Weather forecast-based power predictions and experimental results from photovoltaic systems," in *Power Electronics, Electrical Drives, Automation and Motion (SPEEDAM), 2014 International Symposium on*. IEEE, 2014, pp. 342–346.

[14] Joint Research Centre of the European Commission, "Photovoltaic geographical information system (PVGIS)." [Online]. Available: http://re.jrc.ec.europa.eu/pvgis/apps4/pvest.php

[15] T. Markvart, *Solar electricity*. John Wiley & Sons, 2000, vol. 6.

[16] F. Spertino and J. S. Akilimali, "Are manufacturing I-V mismatch and reverse currents key factors in large photovoltaic arrays?" *IEEE Transactions on Industrial Electronics*, vol. 56, no. 11, pp. 4520–4531, 2009.

[17] F. Spertino and F. Corona, "Monitoring and checking of performance in photovoltaic plants: A tool for design, installation and maintenance of grid-connected systems," *Renewable Energy*, vol. 60, pp. 722–732, 2013.

[18] F. Spertino, F. Corona, and P. Di Leo, "Limits of advisability for master–slave configuration of dc–ac converters in photovoltaic systems," *IEEE Journal of Photovoltaics*, vol. 2, no. 4, pp. 547–554, 2012.

[19] Y. C. Eldar, P. Kuppinger, and H. Bölcskei, "Block-sparse signals: uncertainty relations and efficient recovery," *IEEE Transactions on Signal Processing*, vol. 58, no. 6, pp. 3042–3054, 2010.

[20] B. M. Sanandaji, T. L. Vincent, and M. B. Wakin, "A review on sufficient conditions for structure identification of interconnected systems," *Proceedings of the 16th IFAC Symposium on System Identification*, 2012.

[21] B. M. Sanandaji, "Compressive system identification (CSI): Theory and applications of exploiting sparsity in the analysis of high-dimensional dynamical systems," Ph.D. dissertation, Colorado School of Mines, 2012.

[22] A. Tascikaraoglu, M. Uzunoglu, and B. Vural, "The assessment of the contribution of short-term wind power predictions to the efficiency of stand-alone hybrid systems," *Applied Energy*, vol. 94, pp. 156–165, 2012.

[23] A. Tascikaraoglu and M. Uzunoglu, "A review of combined approaches for prediction of short-term wind speed and power," *Renewable and Sustainable Energy Reviews*, vol. 34, pp. 243–254, 2014.